

A Hybrid Hierarchical Rally Driver Model for Autonomous Vehicle Agile Maneuvering on Loose Surfaces

Manuel Acosta, Stratis Kanarachos and Michael E. Fitzpatrick

School of Mechanical, Aerospace and Automotive Engineering, Coventry University, Coventry, U.K.

Keywords: Agile Maneuvering, Linear Quadratic Regulator, Drift Control, Motion Planning, ADAS.

Abstract: This paper presents a novel Hybrid Hierarchical Autonomous system for improving vehicle safety based on agile maneuvering and drift control on loose surfaces. Standard Electronic Stability Control Systems provide stability by limiting the vehicle body slip, thus reducing the capability of the vehicle to generate lateral acceleration and follow road segments and paths with high curvature on loose surfaces. The proposed system overcomes this shortcoming. Furthermore, it is the first time where a solution for arbitrary road geometries is proposed. The system described in this work consists of three layers. The first layer selects the driver model. The second layer selects the path to be followed and the maneuver type using a Proportional controller and motion planning strategies. The third layer coordinates the steering and driving functions of the vehicle to perform the maneuver, where a Gain-Scheduled Linear Quadratic Regulator is employed to achieve drift control. The hybrid system is implemented in *Matlab/Simulink*® and tested in two scenarios: First, a Rally-like stage formed by a combination of clothoid and arc segments is used to study the drift-path-following capabilities of the system, and lastly, a lateral collision case is proposed to evaluate the suitability of the system as an ADAS Co-Pilot system for lateral collision avoidance.

1 INTRODUCTION

Rallying stands out from other *motorsport* disciplines due to the complexity and peculiarities associated with Rally driving techniques. While *Formula* drivers operate the vehicle linearly, with smooth and gentle inputs, and seeking for quasi-static conditions, professional *Rally* drivers exhibit an aggressive behavior. They take advantage of the car non-linearities and excite the yaw dynamics to generate high yaw accelerations and change the vehicle attitude fast (Blundell and Harty, 2004). It is remarkable how Rally drivers adapt their behavior to the road friction characteristics (e.g. Tarmac, Gravel) and control the vehicle under all kind of disturbances (e.g. roots, bumps). Using an analogy with control systems, it can be stated that *Formula* drivers are very precise controllers for tracking problems (racing line) whereas *Rally* drivers are outstanding robust controllers (drift stabilization).

The problem of off-road autonomous maneuvering has been addressed in (Lenain et al., 2017; Lenain et al., 2012) employing kinematic and dynamic models for low-speed path tracking. In order to develop autonomous vehicles capable of operating the vehicle at higher speeds and more demanding conditions, some authors have focused their research in the study

of the dynamics behind Rally driving techniques. In (Acosta et al., 2016) the yaw acceleration required to perform agile maneuvers such as *Scandinavian Flick* or *Trail Braking* was studied employing the Moment Method Diagram (*MMD*), (Milliken and Milliken, 1995), and a Finite State Machine (*FSM*) capable of performing these tasks autonomously was proposed. In (Velenis et al., 2007) a mathematical analysis of these maneuvers was presented and different trajectory optimization scenarios were studied using a numerical scheme. A stability analysis of aggressive driving techniques was presented in (Yi et al., 2012; Li et al., 2011), and a stability phase portrait based on the yaw rate and the rear wheel slip angle was proposed.

The analysis of drifting techniques was approached in (Hindiyeh, 2013; Velenis et al., 2011; Edelmann and Plochl, 2009). In (Edelmann and Plochl, 2009), the unstable nature of the powerslide motion was studied numerically using a two-track vehicle model and root locus analysis. In (Velenis et al., 2011), the stabilization of a Rear-Wheel-Drive (*RWD*) vehicle around the steady-state drift equilibrium was studied. A cascade control architecture formed by a Linear Quadratic Regulator (*LQR*) and a Backstepping controller was proposed for this purpose. The

same problem was investigated in (Velenis, 2011), but this time a Front-Wheel-Drive (*FWD*) driveline architecture was employed. In (Hindiye, 2013), a nested-loop structure was proposed, and an input coordination scheme was suggested to integrate the lateral and longitudinal control actions.

Finally, the first pieces of evidence of autonomous or semi-autonomous systems that replicate some patterns exhibited by Rally drivers have been found in (Cutler and J.P.How, 2016; Gray et al., 2012). In the former, autonomous drifting is achieved using a methodology to incorporate Optimal Control policies into a Reinforcement Learning (*RL*) process. In (Gray et al., 2012), authors proposed a hierarchical two-level control framework composed of a high-level motion planner and a low-level trajectory tracking controller based on Model Predictive Control (*MPC*).

In this paper, a *Rally-based* driver model is proposed for improving the vehicle safety based on the autonomous execution of agile maneuvers and drift control. The contribution of the paper is significant in what concerns driver modeling, as the drift control action is no longer restricted to constant radius turns and is performed along clothoid and arc segments of different radii instead. In Section 2, the formulation employed to model the vehicle planar dynamics, tires, and road, is presented. In addition, relevant background about the Drift Equilibrium Solutions and Linear Quadratic Optimal Control is provided. The structure of the driver model proposed in this paper is described in Section 3. Simulation results for two scenarios: Rally-like stage and Lateral collision avoidance are provided in Section 4. Finally, conclusions and future intended steps are exposed in Section 5.

2 BACKGROUND

2.1 System Modeling

2.1.1 Single-track Vehicle Model

Following the approach proposed in previous works to study the vehicle behavior in agile maneuvers and drift-equilibrium problems, (Tavernini et al., 2013; Velenis et al., 2010), a single track model is employed in this research, expressions (1-3).

$$\dot{x}_1 = \frac{1}{m}(F_{xf} \cos(u_1) - F_{yf} \sin(u_1) + F_{xr}) + x_2 x_3 \quad (1)$$

$$\dot{x}_2 = \frac{1}{m}(F_{yf} \cos(u_1) + F_{xf} \sin(u_1) + F_{yr}) - x_1 x_3 \quad (2)$$

$$\dot{x}_3 = \frac{1}{I_\psi}(F_{yf} \cos(u_1) l_f + F_{xf} \sin(u_1) l_f - F_{yr} l_r) \quad (3)$$

The vehicle longitudinal velocity (v_x), lateral velocity (v_y), and yaw rate ($\dot{\psi}$), form the state vector of the system ($x = \{v_x, v_y, \dot{\psi}\}$). The terms l_f, l_r correspond to the distance from the front and rear axles to the center of gravity respectively. The vehicle mass is denoted by m and I_ψ is the yaw inertia of the vehicle. The steering wheel angle and the axle longitudinal slips are considered inputs to the system ($u = \{\delta, \lambda_f, \lambda_r\}$). Wheel rotating dynamics modeling is avoided at this stage of the research in order to simplify the problem formulation. The vehicle parameters employed in this paper are presented in Table 1, and correspond to a compact rear-wheel-drive vehicle. The tire forces required to compute the system states are modeled using the nonlinear expressions (4-5).

$$F_{x,i} = F_{z,i} \mu(\lambda_i, \alpha_i), i \in \{f, r\} \quad (4)$$

$$F_{y,i} = F_{z,i} \mu(\lambda_i, \alpha_i) \quad (5)$$

The normal load proportionality principle is assumed, and the tire friction coefficient is presented as a nonlinear function that depends on the axle wheel slips (α) and the axle longitudinal slips (λ). The former are obtained from the geometric equations (6-7), using a small angle approximation (Kanarachos, 2012).

$$\alpha_f = u_1 - \frac{x_3 l_f}{x_1} - \frac{x_2}{x_1} \quad (6)$$

$$\alpha_r = -\frac{x_2}{x_1} + \frac{x_3 l_r}{x_1} \quad (7)$$

Finally, the tire vertical forces (F_z) are calculated using a simple steady-state longitudinal weight transfer model (8).

$$F_{z,i} = F_{z,st} \pm \frac{mh_{CoG}}{l_f + l_r} (\dot{x}_1 - x_2 x_3) \quad (8)$$

The height of the center of gravity is denoted by h_{CoG} , and the static vertical loads are designated by $F_{z,st}$.

Table 1: Parameters of the Single-Track model.

Sym.	Value	Unit	Sym.	Value	Unit
l_f	1.35	m	l_r	1.45	m
h_{CoG}	0.55	m	I_ψ	1800	kgm^2
m	1500	kg	Drive	RWD	—

2.1.2 Tire Friction Model

The tire friction coefficients (μ_x, μ_y) are approximated with a simplified isotropic model that employs a Magic Formula-based (*MF*) formulation. The theoretical longitudinal and lateral slips (σ_x, σ_y), as well as

Table 2: Pacejka tire parameters representative of gravel and asphalt surfaces. (Tavernini et al., 2013).

Surface	B	C	D	E
Gravel	1.5289	1.0901	0.6	-0.95084
Asphalt	6.8488	1.4601	1.0	-3.6121

the equivalent slip (σ) are computed from expression (9), following the formulation presented in (Tavernini et al., 2013; Pacejka, 2012).

$$\sigma_x = \frac{\lambda}{1+\lambda}, \sigma_y = \frac{\tan \alpha}{1+\lambda}, \sigma = \sqrt{\sigma_x^2 + \sigma_y^2} \quad (9)$$

Once the equivalent slip is calculated, the longitudinal and lateral friction coefficients are obtained using equations (10-11).

$$\mu_x = \frac{\sigma_x}{\sigma} D_\lambda \sin[C_\lambda \arctan\{\sigma B_\lambda - E_\lambda(\sigma B_\lambda - \arctan \sigma B_\lambda)\}] \quad (10)$$

$$\mu_y = \frac{\sigma_y}{\sigma} D_\lambda \sin[C_\lambda \arctan\{\sigma B_\lambda - E_\lambda(\sigma B_\lambda - \arctan \sigma B_\lambda)\}] \quad (11)$$

The *MF* tire parameters employed in this paper are shown in Table 2, and were extracted from (Tavernini et al., 2013). These parameters approximate the shape of the friction-slip curves that are characteristic of gravel and asphalt surfaces.

2.1.3 Road Modeling

The position of the vehicle with respect to the reference path is expressed in curvilinear coordinates, (Tavernini et al., 2013). The position of the vehicle along the reference path S_s , the lateral deviation of the vehicle with respect to the road centerline S_n , and the rotation of the vehicle with respect to the road tangent ε , are computed using expressions (12-14).

$$\dot{S}_s = \frac{V \cos(\varepsilon + \beta)}{1 - S_n \kappa} \quad (12)$$

$$\dot{S}_n = V \sin(\varepsilon + \beta) \quad (13)$$

$$\dot{\varepsilon} = \dot{\psi} - \kappa \frac{V \cos(\varepsilon + \beta)}{1 - S_n \kappa} \quad (14)$$

Where κ is the road curvature, V is the module of the velocity, and β is the vehicle body slip angle.

2.2 Drift Equilibrium Solutions

The reference solutions necessary for the drift control task are obtained following the approach presented in

(Velenis et al., 2011). Steady-state conditions are imposed on the vehicle planar motion states, and the vehicle body slip angle (β) and the road radius (R) are fixed. The *Matlab*® function *fsolve* is used to solve the vehicle dynamic equations (1-8). The tire rolling resistance is neglected, and the front axle longitudinal slip is set to zero ($\lambda_f = 0$). In order to study the influence of the tire friction characteristics on the drift equilibrium solutions, the process was repeated using the gravel and asphalt parameters presented in Table 2, and the results depicted in Fig. 1 were obtained.

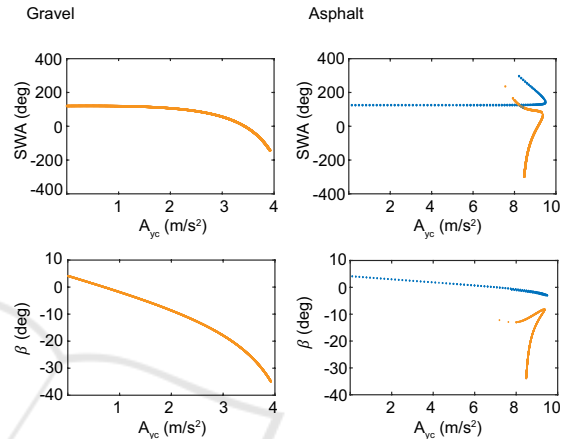


Figure 1: Vehicle Equilibrium Solutions in gravel and asphalt, $R = 20m$. In blue regular solution, in orange drift solution. The steering wheel angle is denoted by SWA and the centripetal acceleration by A_{yc} .

The multiplicity of solutions in asphalt is related to the shape of the friction-slip curve, Fig. 2 right, where a one-to-one mapping between the friction coefficient (μ) and the equivalent slip (σ) does not exist (same friction values can be obtained for small "before-peak" and large "after-peak" slips). A unique equilibrium solution characterized by a large body slip angle at the limit is obtained in gravel, Fig. 1 left. In order to maximize the centripetal acceleration, it is necessary to stabilize the vehicle around a body slip angle of -35 degrees approximately. This change in behavior is due to the different shape of the friction-slip curve in gravel, Fig. 2 left. In this case, the grip scaling approach described in (Pacejka, 2012) and employed to approximate the friction forces in low μ rigid surfaces is no longer valid, and the maximum grip is developed for high slip values.

As can be noticed in Fig. 2 right, the equivalent slips required to achieve maximum centripetal acceleration in asphalt remain close to 0.15 (peak friction force). On the other hand, these values are considerably higher in gravel (0.4-0.7), Fig. 2 left, and have a notable influence on the final equilibrium body slip angle. Results might differ when employing more elaborated tire, chassis, and driveline models, but the

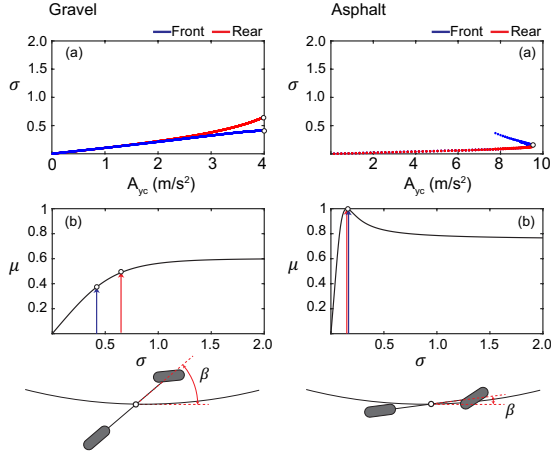


Figure 2: (a) Equivalent slip equilibrium solutions, $R = 20m$. (b) Friction-slip curves for each surface.

physical explanation behind the large drifts exhibited by World Rally Cars (WRC) in Finland or Argentina remains the same.

2.3 Linear Quadratic Regulator

Linear Quadratic Control is often employed in multi-input problems to determine the optimal feedback gain based on the optimization of a performance objective function. In the following, the Infinite Time Horizon case (*LQR*) is presented. For the formulation of the *LQR*, a Linear Time-Invariant (*LTI*) system expressed in state-space form (15) is considered.

$$\dot{\mathbf{x}} = \mathbf{A}\mathbf{x} + \mathbf{B}\mathbf{u} \quad (15)$$

Assuming that the n states of the system are available for the controller, the optimal control vector that stabilizes the plant around the origin is given by the expression (16).

$$\mathbf{u}(t) = -\mathbf{K}\mathbf{x}(t) \quad (16)$$

Where \mathbf{K} is the optimal feedback gain obtained from the optimization of the objective performance function (17).

$$J = \int_0^{\infty} (\mathbf{x}^T \mathbf{Q} \mathbf{x} + \mathbf{u}^T \mathbf{R} \mathbf{u}) dt \quad (17)$$

The terms \mathbf{Q} and \mathbf{R} are positive-definite Hermitian matrices that account for the relative importance of the regulation error and actuator energy expenditure respectively. Substituting the control law (16) in the cost function (17), and following the derivation presented in (Ogata, 2010), the control law can be reformulated as:

$$\mathbf{u}(t) = -\mathbf{R}^{-1} \mathbf{B}^T \mathbf{P} \mathbf{x}(t) \quad (18)$$

Where the constant matrix \mathbf{P} is the unique positive-definite solution to the associated steady-state Riccati equation (19).

$$\mathbf{P}\mathbf{A} + \mathbf{A}^T \mathbf{P} - \mathbf{P}\mathbf{B}\mathbf{R}^{-1} \mathbf{B}^T \mathbf{P} + \mathbf{Q} = 0 \quad (19)$$

The Positive-definite solution of this equation (\mathbf{P}) always exists provided that the matrix $(\mathbf{A} - \mathbf{B}\mathbf{K})$ is a stable matrix (i.e. the closed-loop poles of the system lie on the left side of the complex plane).

2.3.1 Gain-scheduled Linear Quadratic Regulator

In order to implement the *LQR* controller presented previously, the vehicle dynamics equations (1-8) were linearized around the Vehicle Equilibrium Solutions (x_{ss}, u_{ss}). The axle friction forces were linearized using a first order Taylor series expansion (20).

$$\begin{aligned} F_i(\lambda, \alpha) &= F_{i,0} + \frac{\partial F_i}{\partial \alpha} \Delta \alpha + \frac{\partial F_i}{\partial \lambda} \Delta \lambda \\ &= F_{i,0} + C_{i,\alpha} \Delta \alpha + C_{i,\lambda} \Delta \lambda, i \in \{x, y\} \end{aligned} \quad (20)$$

Where the axle longitudinal stiffness ($C_{x,\lambda}$) and the axle cornering stiffness ($C_{y,\alpha}$) were calculated for each equilibrium solution using a finite differences approach (21-22), and the cross-stiffness terms ($C_{x,\alpha}, C_{y,\lambda}$) were neglected.

$$C_{x,\lambda} \approx \frac{F_{x,\lambda_{ss}+\Delta\lambda} - F_{x,\lambda_{ss}-\Delta\lambda}}{2\Delta\lambda} \quad (21)$$

$$C_{y,\alpha} \approx \frac{F_{y,\alpha_{ss}+\Delta\alpha} - F_{y,\alpha_{ss}-\Delta\alpha}}{2\Delta\alpha} \quad (22)$$

The Vehicle Equilibrium Solutions were found for a grid of operating conditions ($\beta_{ss} = \{0 : 5 : 30\}$, $R_{ss} = \{10 : 10 : 400\}$), and the plant (A_{ss}) and input (B_{ss}) matrices obtained after the system linearization were parameterized at each operating point.

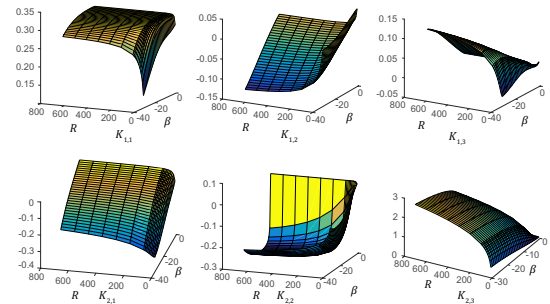


Figure 3: Gain surfaces of the Gain-Scheduled *LQR*.

Finally, the gain surfaces depicted in Fig. 3 were obtained for each operating point. Following the same formulation as (Velenis et al., 2011), the final steering

and rear longitudinal slip control inputs were computed using expression (23).

$$\mathbf{u} = \mathbf{u}_{ss} + \mathbf{K}_{ss}(\mathbf{x} - \mathbf{x}_{ss}) \quad (23)$$

Where the regulation terms are added to the steady-state open-loop inputs (u_{ss}). In order to avoid chattering, the input weighting matrix was set ten times greater than the process weighting matrix ($R = 10Q, Q = I_n$).

3 DRIVER MODEL STRUCTURE

The structure of the driver model proposed in this work is depicted in Fig. 4. A Hierarchical Hybrid modeling approach inspired by previous works (Karimodini et al., 2014) has been followed to combine the path following and drift control tasks. The operation of the hierarchical automaton can be described briefly in the following manner.

- *Supervision Layer*: The driver model is selected depending on the road geometry (radius) and the road friction characteristics. Two driver models are considered in this work: a regular or low body slip driver model, and a drift or high body slip one.
- *Path planning Layer*: Four blocks are distinguished in this layer: Straight Look-Ahead (SLA), Step Transitions (ST), Agile Transitions (AT), and Curved Look-Ahead (CLA). The blocks SLA and CLA compute the look-ahead points necessary for the path following task. A Predictive Trajectory algorithm is employed to minimize the lateral deviation error during fast transitions (change in curvature sign, Agile Transitions) and abrupt radius reductions (e.g. from straight line driving to Hairpin turn, Step Transitions).

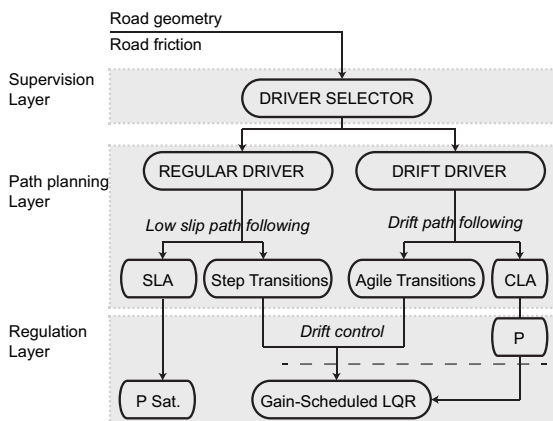


Figure 4: Hierarchical Hybrid Structure, driver model.

- *Regulation Layer*: If the regular driver action is required (straight line or large radius), the steering control action is carried out by a Proportional controller with saturation functions (Casanova, 2000). On the other hand, during lower radius where large body slips maximize the lateral acceleration, Fig. 1, a Gain-Scheduled LQR is used. The tracking references necessary for the regulation task are provided by an upper-level Proportional controller P , which produces an output proportional to the lateral deviation error. Finally, during ST or AT , the drift control action is triggered to change the vehicle heading fast or stabilize the vehicle around a certain body slip.

3.1 Supervision Layer

For simplicity, constant road friction characteristics are considered in this paper, specifically a gravel surface. Thus, the driver model is selected according to the road segment's curvature. During large radii ($R > 400m$) and straight line driving, the low body slip driver is selected. For lower radius where drift is advantageous for maximum centripetal acceleration, the drift driver is used.

3.2 Path Planning Layer

3.2.1 Regular Driver

In the regular driving mode, two blocks are active: SLA and ST.

- *Straight Look-Ahead (SLA)*: This block computes the lateral deviation error of a set of future path coordinates (S_i) considering a straight trajectory, (Casanova, 2000). A proportional controller with saturation functions regulates the path following function (Casanova, 2000).

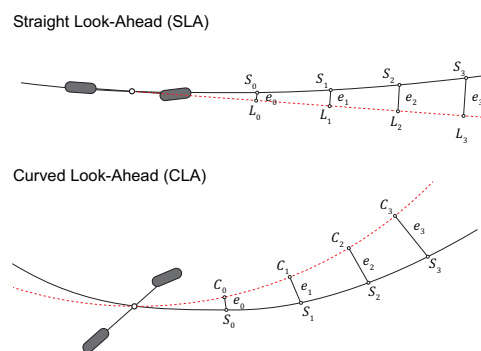


Figure 5: Calculation of the lateral deviation error. Straight Look-Ahead approach (Regular driver) and Curved Look-Ahead approach (Drift Driver).

- **Step Transitions (ST):** The aim of this block is to achieve a fast transition with a minimum lateral deviation between straights and short-radius turns. This behavior is often seen in Rally drivers during *Trail braking* or *Scandinavian Flick* maneuvers, (Acosta et al., 2016), when a high yaw moment is applied to build up a large body slip and initiate the drift condition. In order to model this behavior in the autonomous system, the closed loop response of the Gain-Scheduled *LQR* was computed off-line under a series of Step changes in the reference radius. The trajectories obtained in these tests were normalized and stored in Look Up Tables. The test was repeated for different radii ($R = \{10 : 10 : 400m\}$), and the target body slip during the drift stabilization was set to 20 degrees.

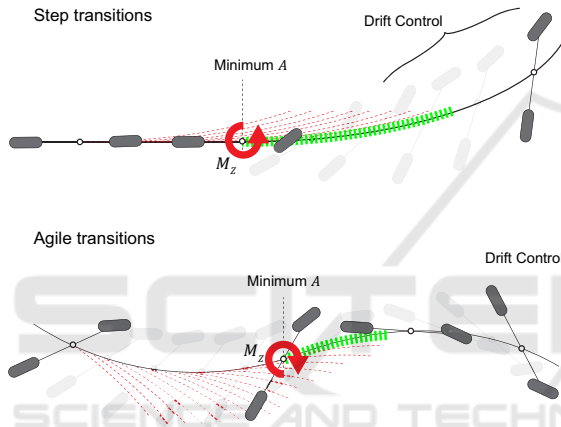


Figure 6: Step transitions and agile transitions. Optimum timing for the application of the yaw moment M_z .

In order to determine the optimum timing to trigger the Step Transition, the area (A) enclosed between the predicted trajectory and the reference path is computed. When the minimum value is found, the step input (yaw moment M_z) is applied and the drift control is switched on. A memory block is employed for this purpose, and the area computed at the current time-step (A_k) is compared to the minimum value calculated in previous steps A_{min} . If the current value is lower, A_{min} is updated. Otherwise, the minimum is found and the Step Transition is triggered. It is assumed that a priori information regarding the arc radius after the transition is available, and thus the trajectory τ_i corresponding to this radius can be selected from the total set of trajectories ($\Omega = \{\tau_{10}, \dots, \tau_{400}\}$). In future investigations, this requirement will be eliminated by evaluating a larger number of candidate trajectories.

3.2.2 Drift Driver

Two blocks are active during the action of the drift driver: *CLA* and *Agile Transitions*.

- **Curved Look-Ahead (CLA):** The action of this block is analogous to the *SLA* block. As the drift driver is active during short radii, it is necessary to consider the curvature of the vehicle trajectory in order to avoid large errors, Fig. 5. The mathematics and geometry involved in the calculation of the lateral deviation error are omitted due to space limitations.
- **Agile Transitions (AT):** The purpose of this block is to concatenate body slip angles of opposite sign with minimum lateral deviation, Fig. 6. This action is performed by Rally drivers when short-radius turns of opposite sign are concatenated (e.g. a sequence of Hairpin Turns). The block is implemented following the same principle than the *ST* block, and the closed loop response of the Gain-Scheduled *LQR* is evaluated off-line for a range of radii. At each radius, the simulation starts in drift equilibrium conditions, with the vehicle body slip stabilized around 20 degrees. The sign of the target body slip is changed suddenly, and the closed-loop response of the system is simulated. The trajectories are then normalized and stored in Look Up tables. At each time-step, the candidate trajectory (τ_i) is translated to the vehicle center of gravity and rotated according to the vehicle heading angle.

**Remark:* As was shown in (Velenis et al., 2011), the body slip at which the lateral acceleration is maximized varies with the radius of the turn. Thus, in order to guarantee minimum time maneuvering it would be necessary to adjust the target body slip angle according to the current radius. For simplicity, it is assumed that near optimal conditions are achieved for a unique target body slip angle.

3.3 Regulation Layer

Two driver models are implemented in the regulation layer: low body slip steering control and high body slip drift control.

3.3.1 Low Body Slip Steering Control

The low body slip steering control was extracted from (Casanova, 2000), and its construction is oriented to racing-line path following problems. In essence, the controller attempts to minimize the heading and lateral deviation errors using proportional gains and saturation functions. The gain values were obtained

from (Casanova, 2000). Concerning the longitudinal control action, a *PID* is employed to track a target speed profile. The generation of the target speed profile is omitted due to space limitations. For simplicity, a constant target speed was considered during the action of the Regular driver.

3.3.2 High Body Slip Drift Control

The function of the high body slip drift controller is more involved, and two blocks are implemented in cascade to achieve the path following and drift control tasks: path following *P* controller and Gain-Scheduled *LQR*, Fig. 7.

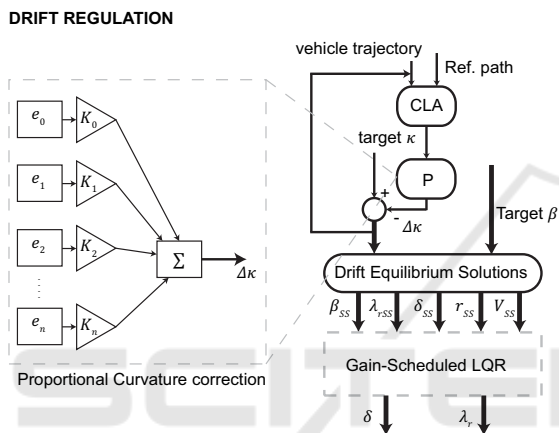


Figure 7: High body slip regulation. Proportional curvature controller and Gain-Scheduled *LQR*.

- **Path Following (*P*) Controller:** As was seen in Section 2.2, for each pair $(\beta_{ss}, \kappa_{ss})$ a set of Vehicle Equilibrium states (x_{ss}) and equilibrium inputs (u_{ss}) exist. In this paper, the path following task is situated in an upper level, and the final target curvature is formed by the reference curvature (κ_{ref}) and a correction term $(\Delta\kappa)$, proportional to the lateral deviation error (24).

$$\kappa = \kappa_{ref} - \Delta\kappa \quad (24)$$

The curvature imposed by the upper level *P* controller is used in combination with the target body slip (β_{ss}) to determine the reference states and reference inputs of the Gain-Scheduled *LQR* $(\beta_{ss}, \lambda_{r,ss}, \delta_{ss}, r_{ss}, V_{ss})$.

- **Gain-Scheduled *LQR*:** This block tracks the reference states (x_{ss}) and inputs (u_{ss}) dictated by the upper level path-following controller, Fig. 7. Details regarding the implementation of this block were provided in Section 2.3.1.

4 RESULTS

4.1 Rally Stage

The driver model was implemented in *Matlab/Simulink*[®] using the vehicle and tire parameters presented in Tables 1 and 2. At this research stage, perfect knowledge of the vehicle parameters, road-friction characteristics, and full state feedback is assumed. The robustness of the controller against uncertainties in the vehicle parameters and road friction characteristics will be addressed in futures stages of this research. A Rally-like stage was constructed using a combination of clothoid, arc, and straight line segments to test the performance of the Hybrid Driver model, Fig. 8.

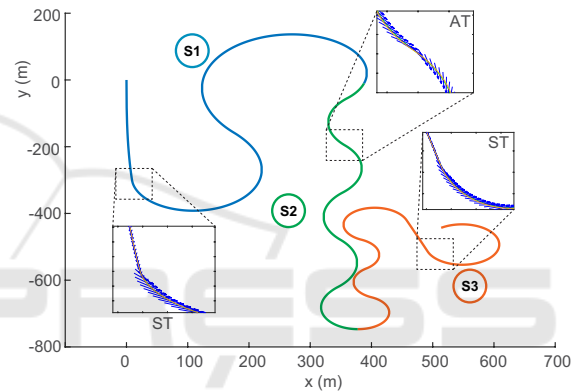


Figure 8: Rally-like segment. Detail of Agile transitions *AT* and Step transitions *ST*.

For simplicity, a target body slip of ± 20 degrees was set during this simulation. Further steps in this research will explore the combination of path following and non-constant body slip tracking. The stage consists of 3 Sectors: *S1*, *S2*, *S3*, and the results obtained in *Matlab*[®] are presented in the following. In order to explain the behavior of the Hybrid system, the following nomenclature has been employed for the *FLAGS* shown in Figures 9-11: (*ST*) Step transitions, (*AT*) Agile transitions, (*P*) Proportional controller ON, (*DRIFT*) Drift driver model ON, and (*REG*) Regular driver model ON. The *LQR* reference signals are denoted as (*Ref*), the Regular driver speed reference by (*REGspd*), and the vehicle states and inputs by (*Sim*).

During the first sector, the vehicle starts in a straight line and executes a *ST* to follow a large left-handed turn ($t \approx 18$). The vehicle is stabilized in *DRIFT* mode and the *P* controller switches on to start the path following task ($t \approx 19.5$). After ($t \approx 40$), an *AT* is performed to track a large right-handed clothoid. The *P* controller is switched off during the

stabilization of the vehicle around the new operating condition and becomes active in ($t \approx 42$) to track the clothoid transition ($R = 200$ to $R = 100$).

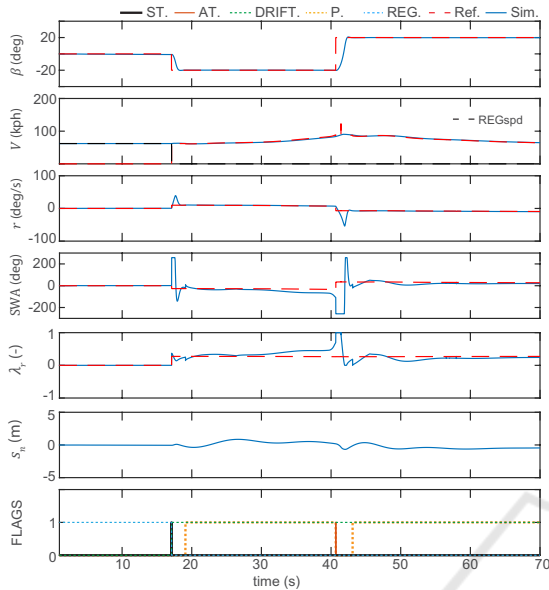


Figure 9: Results of Sector 1.

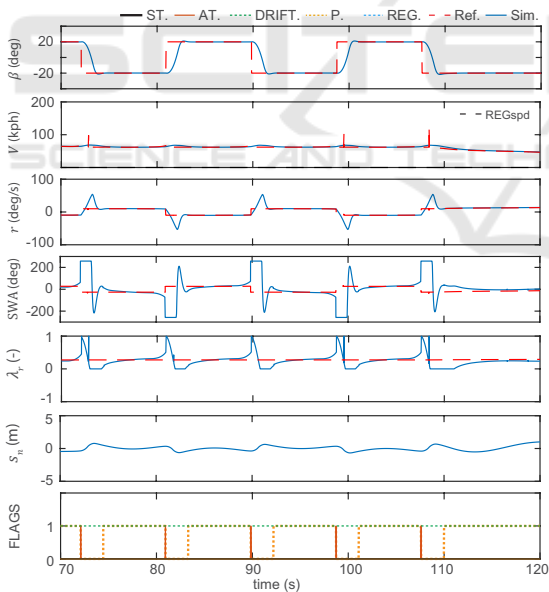


Figure 10: Results of Sector 2.

In the second sector, the system tracks a concatenation of turns. The following sequence (*AT - P OFF - Stabilization - P ON*) is repeated through the sector. As can be noticed in Fig. 10, the Hybrid system generates large yaw accelerations (yaw rate peaks) to change the vehicle attitude fast. This behavior resembles the driving style of Rally drivers (yaw-sideslip excitation, (Blundell and Harty, 2004)), in which the

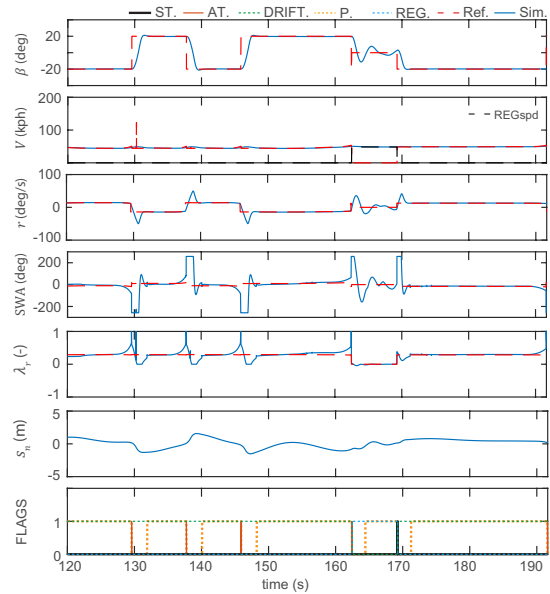


Figure 11: Results of Sector 3.

vehicle is operated in the upper and lower regions of the yaw acceleration versus lateral acceleration plot.

Finally, the results obtained in the third sector are portrayed in Fig. 11. During the first part of the sector, the system tracks a concatenation of $R = 50m$ turns ($t \approx 120$ to $t \approx 150$), followed by a clothoid transition and an arc segment ($R = 60m$). After that, the *REG* driver model switches on to drive the vehicle in the straight segment ($t \approx 165$) and goes off again in ($t \approx 170$) when the *ST* action is triggered. Overall, the Hybrid System exhibited a remarkable performance to track the reference body slip angle with minimum lateral deviation.

4.2 ADAS System for Lateral Collision Avoidance

During the previous subsection, the Hybrid System (Fig. 4) was studied as an entire Autonomous System. In this subsection, however, the system is presented as an *ADAS*, which takes control of the vehicle during critical situations. Now, it is assumed that the responses from the Regular Driver block approximate the behavior of a vehicle equipped with a stability system that tries to mitigate the maximum body slip (i.e. *ESP*, (Zanten, 2002)).

In order to compare the performance of the vehicle equipped with a "traditional" stability system, and that using the proposed *ADAS* system, the test case presented in Fig. 12 is evaluated. The car circulates at a constant speed and approaches a left-handed turn ($R = 50m$) in a gravel surface. An initial test is per-

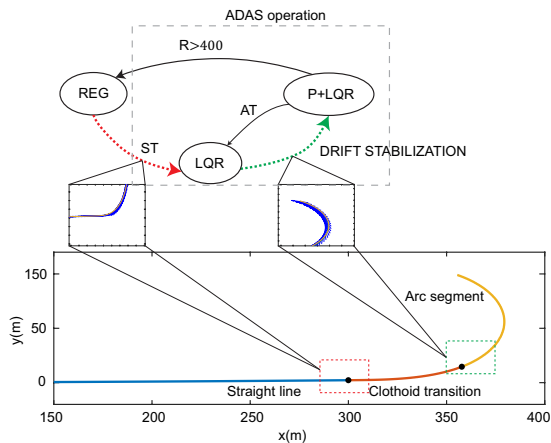


Figure 12: State-Transition diagram of the ADAS hybrid system.

formed switching off the drift driver model (“traditional” stability system) and the same simulation is repeated with the full ADAS system active.

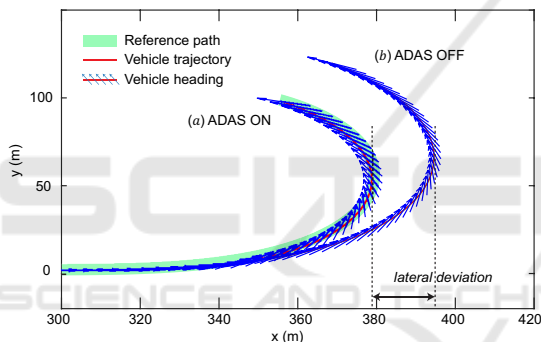


Figure 13: Vehicle trajectories obtained for (a) ADAS ON, (b) ADAS OFF.

As can be noticed in Fig. 13, the vehicle minimizes the lateral deviation when the ADAS system is active. The system triggers the *ST* action, ($t \approx 26.5$, Fig. 14) and switches on the drift control. As was explained in Section 2.2, large body slips are required in gravel in order to maximize the lateral acceleration (Figures 1-2). On the other hand, when the ADAS is OFF and the Regular driver model is active, the latter system tries to minimize the heading error, keeping the vehicle attitude parallel to the tangent of the path (low body slip). This results in a low lateral acceleration, and the vehicle deviates abruptly from the reference path. In order to negotiate the turn, the vehicle should approach the curve with a much lower speed, thus limiting the lateral acceleration demand.

To summarize, when the ADAS system is active, the centripetal acceleration is maximized, and the vehicle can negotiate the turn at a higher speed than when the system is switched off. This could potentially prevent the risk of lateral collision in loose

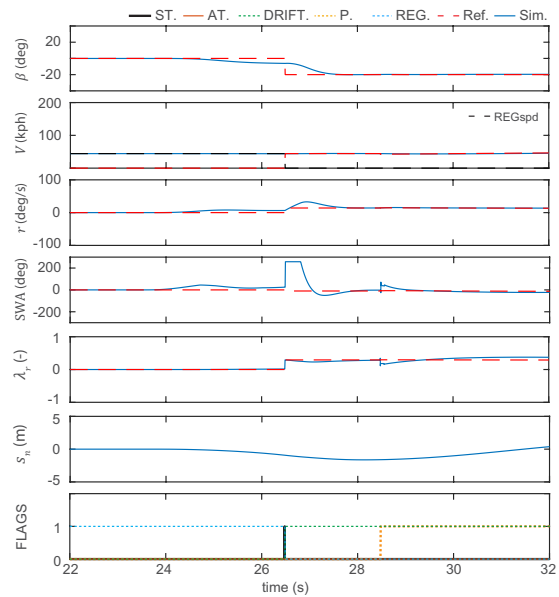


Figure 14: Results obtained with the ADAS ON.

surfaces (deep snow or gravel) when a vehicle approaches a turn at an excessive speed.

5 CONCLUSIONS

In this paper, an innovative Hierarchical Hybrid Driver model for autonomous vehicles has been presented. The aim of the structure is to reproduce the behavior of professional Rally drivers, and employ advanced driving skills such as drift control to enhance vehicle safety when path following is required under tight conditions.

The main contribution of this work is that the drift-like driving control is no longer restricted to constant radius turns, but to complex paths formed by clothoid, arcs, and straight line segments. In order to integrate robustly the body slip control and path following tasks, a hierarchical structure formed by a *P* controller and a Gain-Scheduled *LQR* has been proposed. The path planning modules (Agile transitions) and (Step transitions) have been incorporated in the second layer of the structure, in order to drive the vehicle through a concatenation of turns and alternate the body slip fast with minimum lateral deviation, such as Rally Drivers do.

The system has been implemented in *Simulink*®, and tests have been carried out in a Rally-like stage and a lateral collision scenario. Results evidence the ability of the system to track complex paths while operating the vehicle with large body slips.

Finally, it has been demonstrated that when the vehicle is driven on loose surfaces (centripetal acceler-

ation is maximized with large body slip angles), the drift control action can reduce the risk of lateral collision and prevent the vehicle from lane departure. The refinement of the motion planning algorithms and the evaluation of the robustness of the system under uncertain friction characteristics will be pursued during the next steps of this research.

ACKNOWLEDGEMENTS

This project is part of the Interdisciplinary Training Network in Multi-Actuated Ground Vehicles (ITEAM) European program and has received funding from the European Unions Horizon 2020 research and innovation program under the Marie Skłodowska-Curie grant agreement No 675999. M. E. Fitzpatrick is grateful for funding from the Lloyds Register Foundation, a charitable foundation helping to protect life and property by supporting engineering-related education, public engagement and the application of research.

REFERENCES

- Acosta, M., Kanarachos, S., and Blundell, M. (2016). Agile maneuvering: From rally drivers to a finite state machine approach. In *IEEE Symposium Series on Computational Intelligence*.
- Blundell, M. and Harty, D. (2004). *Multibody System Approach to Vehicle Dynamics*. ELSEVIER Butterworth-Heinemann.
- Casanova, D. (2000). *On minimum time vehicle maneuvering: The Theoretical Optimal Lap, Ph.D Thesis*. School of Mechanical Engineering, Cranfield University.
- Cutler, M. and J.P.How (2016). Autonomous drifting using simulation-aided reinforcement learning. In *IEEE International Conference on Robotics and Automation*.
- Edelmann, J. and Plochl, M. (2009). Handling characteristics and stability of the steady-state powerslide motion of an automobile. *Regular and Chaotic Dynamics*, 14:682–692.
- Gray, A., Gao, Y., Lin, T., Hedrick, K., Tseng, H., and Borrelli, F. (2012). Predictive control for agile semi-autonomous ground vehicles using motion primitives. In *American Control Conference*.
- Hindiyeh, R. (2013). *Dynamics and Control of Drifting in Automobiles, Ph.D Thesis*. Stanford University.
- Kanarachos, S. (2012). A new min-max methodology for computing optimised obstacle avoidance steering maneuvers of ground vehicles. *International Journal of Systems Science*, (45):1042–1057.
- Karimoddini, A., Lin, H., Ben, M., and Tong, H. (2014). Hierarchical hybrid modeling and control of an unmanned helicopter. *International Journal of Control*.
- Lenain, R., Deremetz, M., Braconnier, J., Thuilot, B., and Rousseau, V. (2017). Robust sideslip angles observer for accurate off-road path tracking control. *Advanced Robotics*, 31(9):453–467.
- Lenain, R., Thuilot, B., Cariou, C., Bouton, N., and Berducat, M. (2012). Off-road mobile robots control: an accurate and stable adaptive approach. In *International Conference on Communications, Computing, and Control Applications*.
- Li, J., Yi, J., Zhang, Y., and Liu, Z. (2011). Understanding agile-maneuver driving strategies using coupled longitudinal / lateral vehicle dynamics. In *ASME Dynamics and Control Conference*.
- Milliken, W. and Milliken, D. (1995). *Race Car Vehicle Dynamics*. SAE International.
- Ogata, K. (2010). *Modern Control Engineering*. Prentice Hall.
- Pacejka, H. (2012). *Tire and Vehicle Dynamics*. Butterworth-Heinemann.
- Tavernini, D., Massaro, M., Velenis, E., Katzourakis, D., and Lot, R. (2013). Minimum time cornering: the effect of road surface and car transmission layout. *Vehicle System Dynamics: International Journal of Vehicle Mechanics and Mobility*, 51(10):1533–1547.
- Velenis, A., Katzourakis, D., Frazzoli, E., Tsiotras, P., and Happee, R. (2011). Steady-state drifting stabilization of rwd vehicles. *Control Engineering Practice*, 19(11):1363–1376.
- Velenis, E. (2011). Fwd vehicle drifting control: The handbrake-cornering technique. In *IEEE Conference on Decision and Control and European Control Conference*.
- Velenis, E., Frazzoli, E., and Tsiotras, P. (2010). Steady-state cornering equilibria and stabilisation for a vehicle during extreme operating conditions. *International Journal of Vehicle Autonomous Systems*, 8.
- Velenis, E., Tsiotras, P., and Lu, J. (2007). Modeling aggressive maneuvers on loose surfaces: The cases of trail-braking and pendulum-turn. In *IEEE European Control Conference*.
- Yi, J., Li, J., Lu, J., and Liu, Z. (2012). On the stability and agility of aggressive vehicle maneuvers: A pendulum-turn maneuver example. *IEEE Transactions on Control Systems Technology*, 20(3).
- Zanten, A. (2002). Evolution of electronic control systems for improving the vehicle dynamic behavior. In *International Symposium on Advanced Vehicle Control*.